American Mineralogist, Volume 62, pages 843–865, 1977

Compositional variations of coexisting phases with degree of melting of peridotite in the upper mantle

BJØRN O. MYSEN AND IKUO KUSHIRO[1]

Geophysical Laboratory, Carnegie Institution of Washington
Washington, D. C. 20008

Abstract

A new technique using radioactive tracers has been developed for accurate determination of the degree of melting of rocks. Trace amounts of a compound (CO_2 is used here) or an element that preferentially enters the melt phase are determined. A glass of the starting material is used as standard. The proportion of partial melt equals the ratio of the amount of tracer in the standard and the unknown.

Using this technique, two garnet peridotite nodules, samples 1611 (from a Lesotho kimberlite) and 66SAL-1 (from Hawaiian nephelinite tuff), were subjected to temperatures from their solidi to 1750°C at 20 and 35 kbar pressure. Both peridotite nodules show similar melting behavior. The degree of melting was plotted against temperature, and such melting curves show a distinct change of slope wherever one or more phases disappear. At 20 kbar, olivine (Ol), clinopyroxene (Cpx), orthopyroxene (Opx), and spinel (Sp) coexist with tholeiitic liquid during the initial 25 percent melting of sample 1611 and 60 percent melting of 66SAL-1. The temperature interval of tholeiite melt + 2 pyroxenes + olivine is less than 40°C in both cases.

At 35 kbar, quality chemical analysis of the samples became impossible because of quenching problems. Nodule 1611 begins to melt at about 1625°–1630°C, apparently producing alkali picritic liquid coexisting with garnet, two pyroxenes, and olivine until about 25 percent melting has occurred and the temperature has risen to about 1660°C, where garnet disappears.

The flat slope of the melting curves in the lowest-temperature melting interval and the nearly constant bulk composition of the liquid suggest that the tholeiitic liquid in this melting range may be derived from a peridotitic parent under near isobaric, invariant conditions.

In the lowest-temperature melting interval at 20 kbar two reaction relations between partial melt and crystalline residue are suggested: for 66SAL-1 (lowest temperature) the reaction is Sp + Opx + Cpx (Di_{ss}) $\rightleftarrows$ Ol + Liq; for the higher temperature melting of 1611 the reaction is Ol + Cpx (pigeonite) $\rightleftarrows$ Opx + Liq. The observations suggest that phase equilibria in simple systems such as $MgSiO_3$–$CaSiO_3$–Al_2O_3 and Mg_2SiO_4–$CaMgSi_2O_6$–SiO_2 closely resemble those of natural peridotite in the upper mantle.

Introduction

Accurate determination of the degree of melting of rocks as a function of intensive variables (pressure, temperature, and activity of volatiles) is an important aid to understanding the processes of partial melting and magma genesis. Data on melting behavior of rocks are also useful for understanding major and trace element behavior in liquids and crystals during partial melting and fractional crystallization.

Ever since Bowen (1928) suggested a peridotite source of basalt, genesis of magma by partial melting of peridotitic upper mantle has frequently been discussed either in terms of phase equilibria in appropriate model systems [see Yoder (1976) for discussion and earlier references]. or simply in terms of varying degrees of melting of peridotite compositions (*e.g.*, Green and Ringwood, 1967; Green, 1970). In this study the primary objective was to evaluate these possibilities under volatile-free conditions, although a few experiments involving H_2O are included. Volatiles are important in the upper mantle (for review of data see Irving and Wyllie, 1975; Boettcher *et al.*, 1975; Anderson, 1975). Experimentation in natural and model systems has demonstrated the important

[1] Present address: Geological Institute, University of Tokyo, Hongo, Tokyo 113, Japan.

effects of such components in the partial melting of peridotitic upper mantle (*e.g.*, Kushiro *et al.*, 1968; Kushiro, 1969, 1972; Mysen and Boettcher, 1975a,b; Eggler, 1974, 1975). As a first attempt to study quantitatively the phase equilibria of partial melting of complex natural peridotite, the added complexity of liquid–crystal–vapor equilibria has not been considered.

Experimental technique

Starting materials were two garnet peridotite nodules of the compositions given in Table 1. Nodule 1611 is a sheared garnet peridotite from a Lesotho kimberlite described by Nixon and Boyd (1973). The major element data of Nixon and Boyd (1973) along with the rare-earth element data of Shimizu (1974) indicate that this nodule represents the least depleted upper mantle among kimberlite nodules from South Africa. Preliminary experimental data on sample 1611 were reported by Kushiro (1973). The other nodule, 66SAL-1, is a garnet peridotite from a Hawaiian nephelinite tuff of the Honolulu series first described by Jackson and Wright (1970). Shaw and Jackson (1973) suggested that nodule 66SAL-1 is the most representative of undepleted upper mantle beneath the Hawaiian Islands. Nodule 66SAL-1 has previously been studied at high pressure in the presence of H_2O by Mysen and Boettcher (1975a,b).

Both samples were crushed to less than 5 μm grain size and fired at 1150°C with $f(O_2)$ controlled at the level of the QFM buffer before use. After crushing the original nodule to about 70 μm grain size, a 0.5g split was crushed under acetone for about 90 minutes to reduce the grain size to <5 μm. The heat treatment did not significantly alter the garnet peridotite mineralogy except for a slight tendency toward breakdown of the garnet crystals along their edges. Sample 1611 was also studied with an amount of H_2O equal to that bound in hydroxylated minerals (1.9 weight percent H_2O; Nixon and Boyd, 1973). The hydroxylated minerals are fine-grained phlogopite and serpentine (F. R. Boyd, personal communication, 1976).

Table 1. Compositions of starting materials

	1611*	66SAL-1†
SiO_2	43.70	44.82
TiO_2	0.25	0.52
Al_2O_3	2.75	8.21
Fe_2O_3	1.38	2.07
FeO	8.81	7.91
MnO	0.13	0.19
MgO	37.22	26.53
CaO	3.26	8.12
Na_2O	0.33	0.89
K_2O	0.14	0.03
H_2O^-	0.05	0.11
H_2O^+	1.94	0.15
P_2O_5	tr.	0.04
Cr_2O_3	0.28	0.20
NiO	n.d.	0.20
Totals	100.24	99.99

*Analysis from Nixon and Boyd (1973).
†Analysis from Mysen and Boettcher (1975a).
Both analyses of unfired samples. The analysis of 1611 corresponds to 1611 + 1.9 weight percent H_2O in the text.

The degree of melting of a rock can be determined by adding a trace amount of a compound (*e.g.*, CO_2) that enters only the liquid phase. The partition coefficient of CO_2 between liquid and crystals exceeds 1000 (Mysen *et al.*, 1976), and this compound was therefore selected for this purpose. To this end, approximately 50 ppm CO_2 (as $BaCO_3$) with a known amount of radiogenic ^{14}C was added to each sample. The amount of melt in the sample was determined by beta-track counting of unknown and standard, utilizing the ^{14}C spike as described by Mysen and Seitz (1975). The standard was a glass of the starting material with ^{14}C-spiked CO_2 added. The percentage of melt in the unknown is then simply

$$\text{percentage melt} = [(\text{carbon in all glass standard})/(\text{carbon in glass of partially melted unknown})] \times 100 \quad (1)$$

More than 2 weight percent CO_2 dissolves in basaltic melts at pressures above 20 kbar (Mysen *et al.*, 1975). Therefore, with 50 ppm CO_2 added to the sample, no CO_2 vapor will be present in equilibrium with CO_2-saturated partial melt when the amount of melt is larger than 0.25 percent. The absence of vapor is a requirement for accurate determination of the percentage of melt in a charge when using ^{14}C-spiked CO_2 as the analytical tool. In sample 1611 + 1.9 weight percent H_2O, this requirement presented a problem inasmuch as H_2O-rich vapor may be present in the 5–10 percent melting range. No modifications of the technique were made to overcome this problem, however, because of the relatively slight importance assigned to this part of the system in the present experiments. In general, the problem can be solved by changing to another radioactive isotope that does not dissolve in vapor and does not enter crystalline silicates in significant amounts (*e.g.*, tungsten-185).

Carbon dioxide is formed in the experiment by breakdown of finely-disseminated $BaCO_3$ during heating prior to melting of the sample. Mysen and Seitz (1975) have shown that a run duration of 5 minutes is necessary to attain equilibrium CO_2 con-

tents of a silicate liquid of albite composition at 1450°C and 20 kbar. Because the present experiments were at similar temperatures and the run durations far exceeded 5 minutes (Table 2), equilibrium was in all likelihood attained.

The uncertainties in the data include the counting statistics, heterogeneities of carbon in the samples, and the exposure times. As seen from the data in Table 2, the total relative uncertainty ($\pm 1\sigma$) is generally less than 5 percent.

Crystallization of quench phases (pyroxene and olivine) is sometimes a problem in chemical analysis of the phases present in the experiments. Fortunately, carbon remains in the quench minerals at least on an optical scale (needed for beta-track counting). This occasional problem therefore did not affect the results of the determination of the degree of melting.

All experiments were carried out in a solid-media, high-pressure apparatus similar to the design of Boyd and England (1960). The experiments were done by the piston-out technique with no correction for friction, resulting in ±1.5 kbar uncertainty. Temperatures were measured with Pt-Pt90Rh10 thermocouples without pressure correction on emf output. The absolute accuracy of the temperature measurements is about ±10°C. However, the automatic temperature controllers maintain the nominal temperatures to within 3°C, which is probably the approximate precision in these experiments. Consequently, temperature effects could be observed within about 5°C.

The samples were contained in sealed $Pt_{95}Au_5$ containers. Sealed capsules were used to avoid loss of carbon dioxide. Glass-sleeved furnace assemblies of 0.5 inch diameter were used in all experiments to minimize access of hydrogen (from H_2O released from the outer talc sleeve) to the sample area. This experimental configuration was employed to reduce the iron loss to the capsule by reducing the effect of hydrogen fugacity on the oxidation state of iron inside the capsule. However, the $Pt_{95}Au_5$ capsules still dissolved sufficient iron to result in about 20 percent

Table 2. Data on experimental runs

Run No.	Temp. (°C)	Pressure (kbar)	Run Duration (min.)	Phases Present	Percent Melt
			Starting Material 66SAL-1		
4-49	1350	20	240	Ol, Opx, Cpx, Sp, Liq	1.49 ± 0.07
4-57	1363	20	190	Ol, Opx, Cpx, Sp, Liq	11.5 ± 0.6
4-45	1375	20	180	Ol, Opx, Cpx, Sp, Liq	59.7 ± 1.8
4-50	1400	20	120	Ol, Opx, Liq	85 ± 5
4-59	1500	20	60	Ol, Liq	97 ± 2
			Starting Material 1611 + 1.9 weight percent H_2O		
4-84	1460	20	180	Ol, Opx, Cpx, Liq	6.1 ± 0.3
4-70	1475	20	180	Ol, Opx, Cpx, Liq	13.5 ± 0.5
4-62	1500	20	105	Ol, Opx, Cpx, Liq	33.5 ± 1.5
4-74	1525	20	120	Ol, Opx, Liq	39.6 ± 1.5
4-81	1550	20	210	Ol, Liq	59 ± 3
4-72	1600	20	60	Ol, Liq	60.3 ± 2.7
4-71	1750	20	5	Ol, Liq	73.7 ± 3.7
			Starting Material 1611		
4-109	1450	20	180	Ol, Opx, Cpx, Liq	1.32 ± 0.04
4-110	1475	20	180	Ol, Opx, Cpx, Liq	1.77 ± 0.05
4-114	1500	20	180	Ol, Opx, Cpx, Liq	15.7 ± 0.5
4-127	1525	20	150	Ol, Opx, Liq	28.5 ± 0.7
4-119	1550	20	120	Ol, Opx, Liq	34.5 ± 0.8
4-129	1600	20	75	Ol, Liq	44.1 ± 1.5
4-131	1700	20	75	Ol, Liq	60.8 ± 1.2
412	1610	35	90	Ol, Opx, Cpx, Ga, Liq	0.69 ± 0.01
411	1625	35	90	Ol, Opx, Cpx, Ga, Liq	0.92 ± 0.02
409	1650	35	70	Ol, Opx, Cpx, Ga, Liq	13.6 ± 0.3
414	1663	35	90	Ol, Opx, Cpx, Ga, Liq	23.9 ± 0.5
413	1685	35	60	Ol, Opx, Cpx, Liq	43.6 ± 1.0
408	1700	35	30	Ol, Opx, Liq	44.5 ± 1.2
410	1750	35	20	Ol, Opx, Liq	61.4 ± 1.0

iron loss from the samples at 20 kbar pressure at the highest temperatures (>1550°C). The iron loss was considerably higher at 35 kbar. This increase at higher pressure is ascribed to the much lower viscosity of silicate liquids at 35 kbar compared with 20 kbar (65 percent decrease; Kushiro *et al.*, 1976), resulting in higher diffusion rates and therefore more rapid transport of iron from the charge to the capsule. Alternatives to simple noble-metal capsules, such as graphite capsules inside platinum capsules, had to be discarded because of exchange of ^{14}C between graphite and the silicate charge. Consequently, it was decided to accept the iron loss, even though that problem may produce uncertainties in applying variation of iron content during the experiments. For example, 20 percent iron loss in olivine results in ~1 percent increase of Fo content with Fo_{90} composition. Such uncertainties are much smaller than the observed temperature effects and therefore do not affect the conclusions significantly.

All analytical data were obtained with the MAC automated electron microprobe at the Geophysical Laboratory using 15 kV acceleration voltage. Quenched liquids (glass) were analyzed with 0.01 μA beam current to reduce loss of alkalies by volatilization. The data show that even with such precautions, 50 percent or more Na_2O and some K_2O were lost from the glasses. However, no further attempts were made to correct the alkali loss in the analyses presented.

Results

Phase equilibria

Data on the experimental runs appear in Table 2. Degree of melting [X(melt)] is plotted against temperature (T) for nodules 1611 and 66SAL-1 at 20 kbar in Figure 1. The model composition $Fo_{55}En_{30}Di_{15}$ (by weight), used to illustrate melting behavior of simple systems in this kind of diagram, is representative of typical peridotite.

The identification of phase fields as presented in the figures is based on optical data and confirmation by the electron microprobe. Whether spinel occurs together with olivine and two pyroxenes in sample 1611 (Fig. 1) is uncertain. A few grains $\lesssim 1$ μm across and apparently isotropic, may be spinel, but this observation could not be confirmed with the electron microprobe. Spinel is therefore left out of the figure. Clinopyroxenes are called Ca-rich or Ca-poor on the basis of their chemical compositions. Kushiro (1969) and Kushiro and Yoder (1970) suggested that pigeonite is stable to at least 20 kbar. Some, if not all, of the Ca-poor clinopyroxenes in 1611 could be pigeonite (see discussion below), whereas all the clinopyroxenes of 66SAL-1 are Ca-rich (diopsidic).

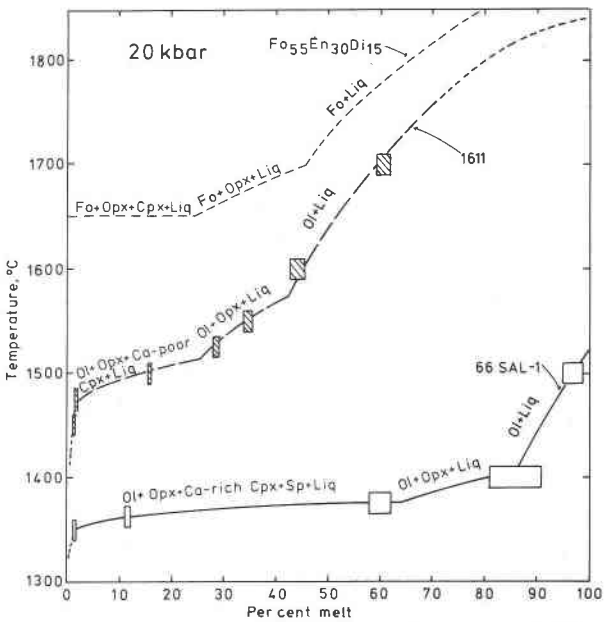

Fig. 1. Melting curves of nodules 1611 and 66SAL-1 at 20 kbar pressure (anhydrous). Size of boxes includes uncertainties in temperature (±10°C) and determination of percentage of liquid ($\pm\sigma$). $Fo_{55}En_{30}Di_{15}$ curve from Kushiro (1969).

Starting from the solidi (Fig. 1), the melting ranges of these peridotites are divided into three distinctly different fields, olivine + 2 pyroxenes + liquid (+ spinel), olivine + orthopyroxene + liquid, and olivine + liquid. There is also a striking similarity between these patterns and that of composition $Fo_{55}En_{30}Di_{15}$ in the three-component system Di–Fo–SiO_2 (Kushiro, 1969). Solid solutions involving Fe, Al, Cr, and Na in the natural samples do, of course, result in slightly different curvature of the melting curves of the natural samples compared with that of the simple system. The initial melting step (Ol + 2 Px [+ Sp] + Liq) of both 1611 and 66SAL-1 closely resembles the invariant melting behavior of the synthetic composition (Fig. 1), suggesting that volatile-free melting of natural peridotite may approximate an invariant character. Both melting curves of the natural rocks show a sharp dip close to their solidi without change of phase assemblage. This feature does not occur in the simple system. Both nodules contain several tenths of a percent alkalies. It may be that such cations (chainbreakers or depolymerizers [Bottinga and Weill, 1972; Waff, 1975]) in-

duce a small amount of melting at a considerably lower temperature than in their absence. Qualitatively, this melting behavior resembles that of H_2O-deficient rocks in the absence of hydrous minerals (as defined by Merrill *et al.*, 1970). Clearly, the melting is not invariant in this region.

The solidus temperature of rock 1611 was reported as 1475°C at 20 kbar by Kushiro (1973). If the melting curve of 1611 in Figure 1 is extrapolated linearly from temperatures immediately above the sharp dip, the solidus temperature also becomes 1475°C. Similarly, the solidus of 66SAL-1 becomes 1350°C at 20 kbar.

Samples 1611 and 66SAL-1 are quantitatively different in terms of temperature and degree of melting at which phase changes occur. The degree of melting of sample 66SAL-1 increases from 1.5 to 60 percent between 1350° and 1375°C at 20 kbar without change of phase assemblage. In comparison, only 25 percent melt can be derived from 1611 before clinopyroxene disappears (Fig. 1).

Water-free and water-undersaturated melting of 1611 at 20 kbar is shown in Figure 2. The presence of a small amount of water in 1611 adds two technical problems. First, as discussed above, vapor may occur as a separate phase at the lowest degree of melting (the partial melt of 1611 + 1.9 weight percent H_2O is probably water-saturated with the degree of melting below about 7 percent). Under such conditions some carbon dioxide partitions into the H_2O-rich vapor, and the amount of CO_2 left in the partial melt is less than that for a similar proportion of melt under water-free conditions. Consequently, the 6.1 percent melting shown in Figure 2 may be an overestimate. Second, the presence of quench minerals, forming more readily from hydrous silicate melt, results in greater difficulty in analyzing the run products of 1611 + 1.9 weight percent H_2O. The two melting curves obtained with nodule 1611 at 20 kbar (H_2O-free and with 1.9 weight percent H_2O) are quite similar, except that the hydrous curve lies at lower temperatures. The temperature difference increases from 25°C within the olivine + 2 pyroxene + liquid field to more than 150°C at 60 percent melting. The difference in the degree of melting at a given temperature inside the melting range where pyroxene is present is as much as 25 percent (absolute) because of the flat slope of the melting curves in this temperature region.

The results from sample 1611 at 20 and 35 kbar pressure are shown in Figure 3. The melting interval at 35 kbar can be subdivided into four distinct regions, although the highest-temperature field in Fig-

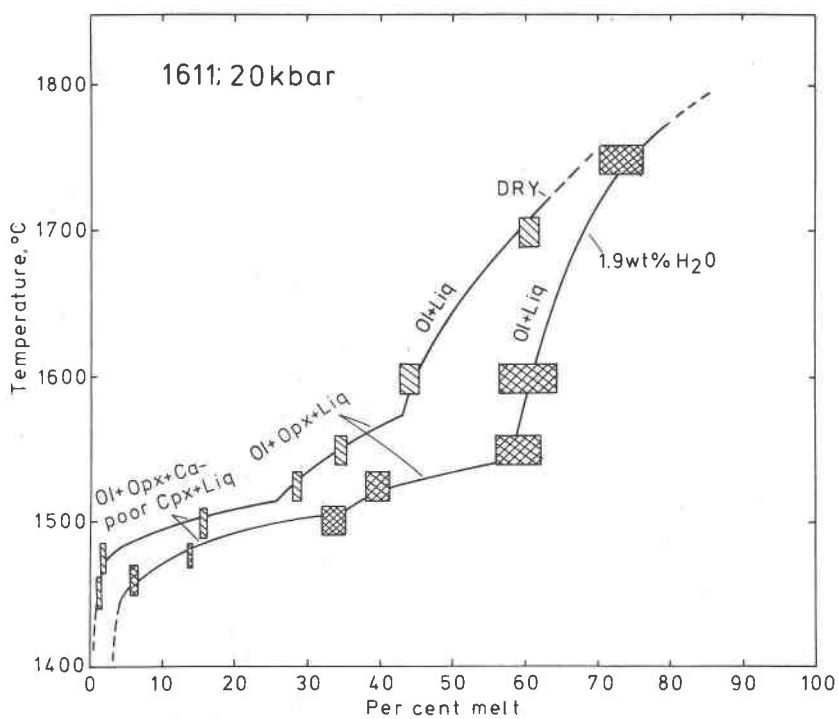

Fig. 2. Melting curves of 1611 anhydrous and in the presence of 1.9 weight percent H_2O at 20 kbar. Size of boxes as in Fig. 1.

ure 3 was not determined. The stippled line and the bracketed "Ol + Liq" field are merely a suggestion, constrained only by the improbability of the 35 kbar melting curve intersecting the 20 kbar melting curve.

The phase assemblages at 35 kbar are different from those at 20 kbar in two respects. First, garnet appears on the 35 kbar solidus and remains stable to about 25 percent melting. Apart from the sharp dip below about 1 percent melting, the interval of garnet stability is about 40°C. Second, pyroxene has a much wider stability interval at 35 kbar than at 20 kbar (to ~60 and 45 percent melting, respectively, at 35 and 20 kbar; Fig. 3). Because of the steeper slopes of the 20-kbar melting curve, the individual intervals include about the same amount of melt (excluding, of course, the interval of garnet stability, which has no 20-kbar analogue). The melting intervals above that of garnet stability involve the same minerals as those at 20 kbar (Fig. 3).

The ambiguity of the solidus temperature at 35 kbar is the same as at 20 kbar. Extrapolation of the 35 kbar melting curve similar to that of the 20 kbar melting curve results in a solidus temperature of 1625°–1630°C for 1611. The data of Kushiro (1973), extrapolated linearly from 25 kbar, suggest 1660°C as the 35 kbar solidus temperature.

Analytical data

Reliable chemical data were obtained on samples held at 20 kbar. Quenching problems became increasingly cumbersome as pressure, temperature, and H_2O and alkali contents of the system increased. The most common quench mineral is an olivine (~43 weight percent SiO_2) with 2–4 weight percent Al_2O_3 and CaO (submicroscopic liquid inclusions?) and with Mg/(Mg + Fe) = 0.89–0.90. Quench olivine is commonly optically indistinguishable from stable olivine, and its identification is based mostly on its chemical composition. The hydrous runs also resulted in quench clinopyroxene containing ~10 weight percent CaO and ~10 weight percent Al_2O_3 and having Mg/(Mg + Fe) = 0.7–0.75. The presence of significant amounts of such quench clinopyroxene in sample 1611 + 1.9 weight percent H_2O made it particularly difficult to obtain reliable analyses of Ca-poor clinopyroxene from this sample. Similar quench pyroxene precipitated from liquids of sample 66SAL-1, but because of the greater compositional difference between stable and quench clinopyroxene in this material, reliable data could be obtained. Analysis of quenched liquid (glass) from H_2O-free 1611 was simpler because the main quench mineral was olivine. The total CaO and Al_2O_3 contents of liquids increased dramatically in liquid volumes supplying components to such quench minerals. Quality liquid analysis could be obtained by moving the electron beam away from the quench mineral until the CaO and Al_2O_3 contents of the quenched glass were lowered to a fixed value.

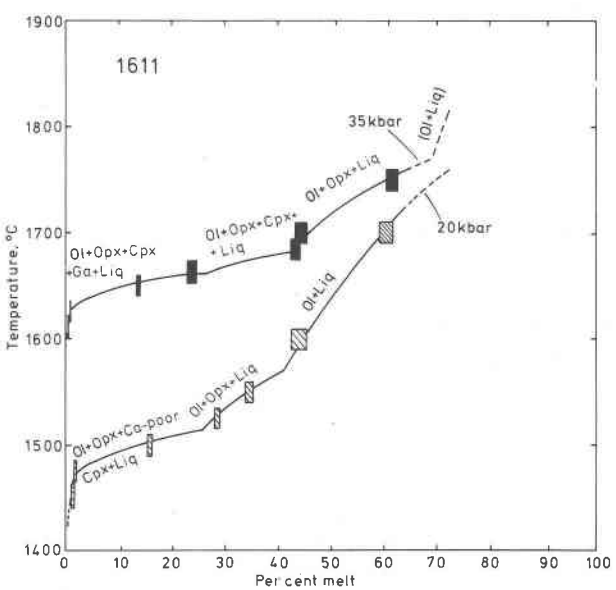

Fig. 3. Melting curves of nodule 1611 at 20 and 35 kbar (anhydrous). Size of boxes as in Fig. 1.

All experiments at 35 kbar underwent very extensive quench-mineral crystallization, including both olivine and two pyroxenes. The problem proved sufficiently severe to abort attempts to obtain quality analytical data from such experimental run products.

Olivine. Relevant olivine compositional trends for both nodules as a function of degree of melting are shown in Figure 4. Their Mg/(Mg + Fe) (Fo content) define the same distinct melting ranges as shown by the melting curves (Figs. 1 and 2). The most rapid changes of Fo content occur just above the peridotite solidus and in the olivine + liquid fields, suggesting the largest participation of olivine in the melting reactions in these melting ranges. The Fo content decreases particularly rapidly close to the peridotite solidus. Iron loss to the capsule after significant amounts of melt have formed may, however, partially account for the rapid change of Fo content.

Spinel. Spinel data from nodule 66SAL-1 are plotted in Figure 5. Spinel is the most Cr-rich phase among the minerals encountered in these experiments, containing up to 3.26 weight percent Cr_2O_3 at 1375°C and 20 kbar. The Cr/(Cr + Al) of spinel

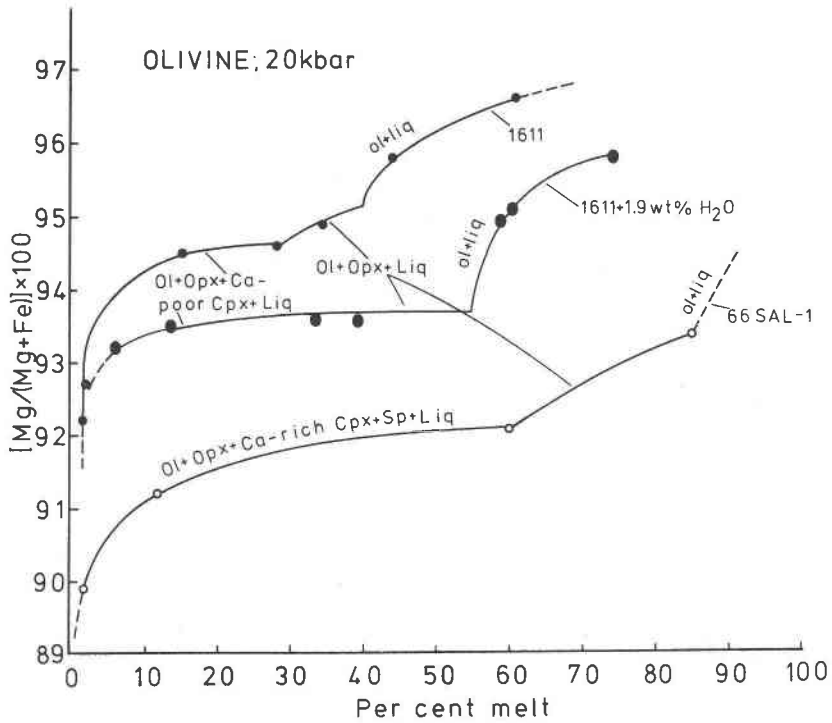

Fig. 4. Chemical trends of olivines as a function of degree of melting. Mineral assemblages describe coexisting phases in melting intervals.

increases smoothly with increasing degree of melting. Similar observations were reported by Mysen and Boettcher (1975b) for spinels from 66SAL-1 at about 1000°C in the presence of H_2O-saturated liquid. The Mg/(Mg + Fe) of spinel also increases smoothly with increasing degree of melting (Fig. 5B). Like olivine (Fig. 4), spinel releases its Fe component most rapidly during the initial stages of melting.

Orthopyroxene. Relevant chemical data for orthopyroxene are shown in Figures 6 and 7. The Mg/(Mg + Fe) of this pyroxene as a function of degree of melting (Fig. 6A) defines the phase fields much like that of olivine (Fig. 4). Furthermore, Fe–Mg change during melting is most rapid in the beginning of each melting range and with the fewest phases present. In contrast, alumina content does not follow such a simple pattern (Fig. 6B). Orthopyroxene of the aluminous sample 66SAL-1 contains three to four times more Al_2O_3 in its melting range than does that of 1611. The melting range of 66SAL-1 is about 100°C lower than that of 1611, probably contributing to this difference. The coexisting clinopyroxene may also be different in 66SAL-1 and 1611, owing to the lower temperatures of the 66SAL-1 melting range (see below). Furthermore, the melting behavior of orthopyroxene of 1611 depends on the presence of H_2O. The orthopyroxene of 1611 + 1.9 weight percent H_2O shows continuously-decreasing alumina content, whereas the Al_2O_3 of orthopyroxene of H_2O-free 1611 remains constant within the two melting ranges where it is stable (Figs. 1, 2, and 6B). The chromium content of orthopyroxenes is generally low ($\leq$0.5 weight percent Cr_2O_3) and their Cr/(Cr + Al) define phase fields much like those defined by Mg/(Mg + Fe) (Figs. 6A and C).

The compositions of coexisting pyroxenes are plotted in the pyroxene quadrilateral in Figure 7. The end members (En, Fs, and Wo) are simply Fe:Mg:Ca ratios. This procedure of calculation was adopted because the Fe^{3+}/Fe^{2+} of the pyroxenes are not known and the amounts of various Tschermak's molecules could not be calculated from the analyses. The effect of this simplification on the orthopyroxenes is relatively small. Their position in the quadrilateral is temperature-dependent. The amount of melt is unimportant as long as the clinopyroxene is present. However, the Wo component decreases rapidly and the En component increases after the clinopyroxene is absorbed in the melt.

Clinopyroxene. Relevant analytical data are plotted

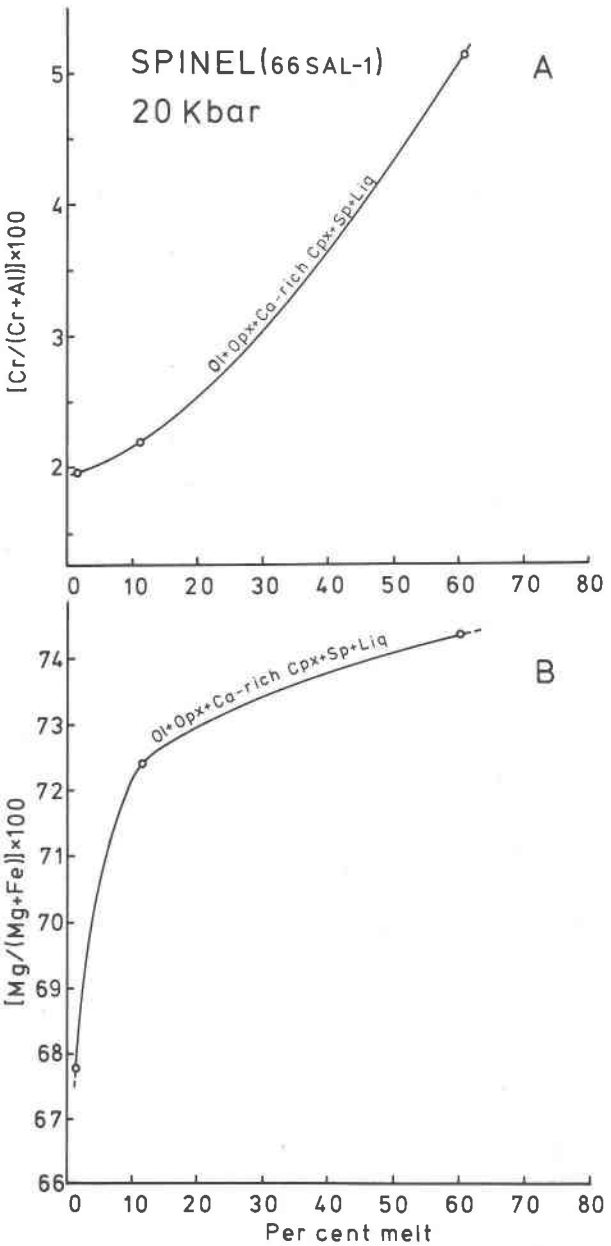

Fig. 5. Chemical trends of spinels from nodule 66SAL-1. Mineral assemblages describe coexisting phases in melting intervals.

in Figures 7 and 8. Apparently, there is a crystal-chemical difference between the clinopyroxenes of sample 66SAL-1 on the one hand and those of 1611 on the other (Fig. 7). The clinopyroxenes from 1611 (high-temperature melting interval) have only about half the amount of Wo solid solutions that the 66SAL-1 clinopyroxenes have (15–20 and 40–50 mole percent, respectively). Furthermore, the clinopyroxenes from 1611 are more iron-rich than those from 66SAL-1 (Fig. 8A), despite the higher temperature of formation and the more magnesian coexisting crystalline phases of 1611 (Figs. 4, 6, 7, and 8). The Wo content of clinopyroxene is simply [Ca/(Ca + Mg + Fe)] × 100. However, about 10–14 percent of the tetrahedral cations in both 66SAL-1 and 1611 clinopyroxenes is occupied by aluminum. This Al^{IV} may be subtracted as $CaAl_2SiO_6$, leaving less than 5 percent wollastonite in 1611 clinopyroxene, or it may be shared between (Mg, Fe, Ca, and Ca–Ti) Tschermak's molecules, yielding more than 5 mole percent Wo. The net result is a Ca-clinopyroxene resembling pigeonite. The data of Kushiro and Yoder (1970) and Hensen (1973) suggest between 10 and 15 mole percent wollastonite component in pigeonite in this pressure and temperature range. In that case, 50–75 percent of Al^{IV} is present in these clinopyroxenes as (Mg,Fe) Tschermak's molecule. The Mg–Fe partitioning between coexisting pyroxenes of 1611—$[Mg/(Mg + Fe)]_{opx}/[Mg/(Mg + Fe)]_{cpx}$ = 1.11–1.14—is in close agreement with the experimental data on coexisting enstatitic and pigeonitic pyroxenes by Hensen (1973) and with data on natural coexisting orthopyroxene and pigeonite by Kushiro and Nakamura (1970), further substantiating the identification of the Ca-poor clinopyroxene from 1611 as pigeonite. Quality analysis of Ca-poor clinopyroxenes from 1611 + 1.9 weight percent H_2O could not be obtained because of significant interference from quench pyroxene. Semi-quantitative compositional data resemble those for clinopyroxenes from experiments with anhydrous 1611.

The clinopyroxenes from 66SAL-1 are diopsidic. The difference between these two samples is simply the result of the temperature difference of their 20 kbar melting intervals (1450°–1500°C and 1350°–1375°C respectively, for 1611 and 66SAL-1). Kushiro and Yoder (1970) determined the lower stability limit of iron-free pigeonite in the diopside–enstatite join to be 1450°C at 20 kbar, in close agreement with the data shown in Figures 7 and 8.

The overall chemical trends (Fig. 8) are qualitatively similar for Ca-rich pyroxenes from 66SAL-1 and 1611. Both gain Mg and Cr and lose Wo and Jd components (Figs. 8B and D) with increasing degree of melting (Figs. 8A and C). Similar results were obtained by Mysen and Boettcher (1975b) for diopsidic pyroxene of 66SAL-1 in the presence of H_2O-saturated liquid at about 1000°C.

Liquid. Liquid compositions at 20 kbar are shown in Table 3. The liquids can be classified into three

major groups (excluding the compositions within the first few percent of melting). The melt coexisting with olivine + 2 pyroxenes is olivine tholeiitic, followed by picritic melt coexisting with olivine + orthopyroxene and komatiitic (perioditic) melt coexisting with olivine alone. Melts of both 66SAL-1 and 1611 at <2 percent melt (within the dip of the melting curves; Figs. 1 and 2) are nepheline-normative, with normative nepheline contents decreasing from 7.6 percent at 1.32 percent melt (1611) to 4.7 percent at 1.77 percent melt (Table 3). The phase assemblage does not change as the liquid composition changes from nepheline- to olivine- and hypersthene-normative at higher degrees of melting. The analytical data for coexisting minerals, particularly the alkali content of clinopyroxene (Fig. 8B), suggest that such readjustments of solid solutions are the major contributing factors in the formation of nepheline-normative liquids in this low degree-of-melting range.

Variations of individual oxide contents of liquids plotted against degree of melting are shown in Figure 9 for SiO_2, Al_2O_3, and CaO. In this figure, compositional changes over changes in phase assemblage are drawn as straight vertical lines. Liquid compositions must change continuously, though rapidly, in such regions. Because the nature of these changes is not known, the compositions are simply connected with straight lines in Figure 9.

Figure 9A shows how the silica content of 1611 liquids remains constant up to 45 percent melt, owing to the presence of pyroxene(s) of relatively constant silica content. After pyroxene is lost, the liquids rapidly lose SiO_2, approaching komatiite composition. The temperature at 20 kbar is about 1550°C for 1611 at this point. The presence of 1.9 weight percent H_2O depresses this situation to 1525°C and 60 percent melting. This increase in degree of melting in the presence of some H_2O is to be expected, from data on relevant H_2O-bearing systems (*e.g.*, Kushiro *et al.*, 1968). If 66SAL-1 can be treated as possible source material for upper mantle magma, peridotitic komatiite may be produced at 85 percent melting at temperatures as low as 1400°C.

The alumina contents of liquids are plotted in Figure 9B and are controlled by the presence of highly aluminous clinopyroxene (7–9 weight percent Al_2O_3). After the alumina-rich crystalline phase is melted, the alumina content of the liquids drops rapidly and is essentially a function of the amount of crystals left in the system.

The calcium contents of 1611 liquids (Fig. 9C) are interesting because the Ca content of coexisting cli-

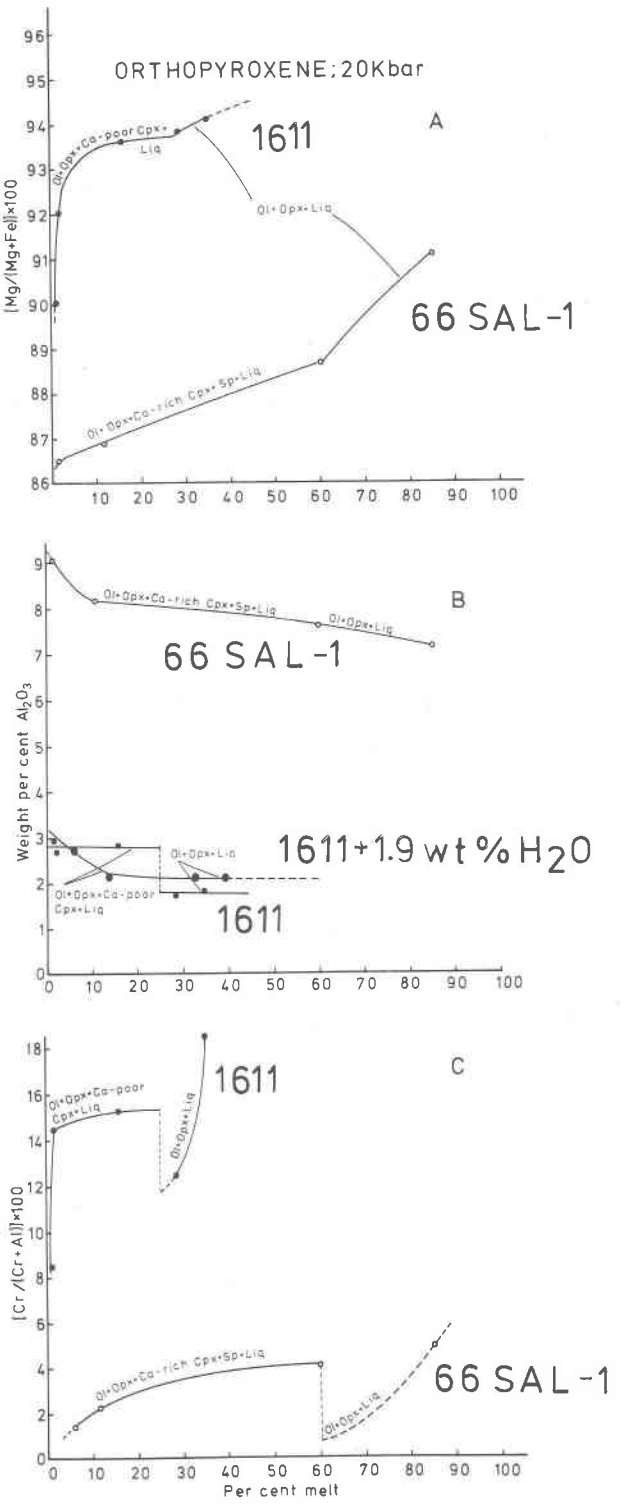

Fig. 6. Chemical trends of orthopyroxenes as a function of degree of melting. Mineral assemblages describe coexisting phases in melting intervals.

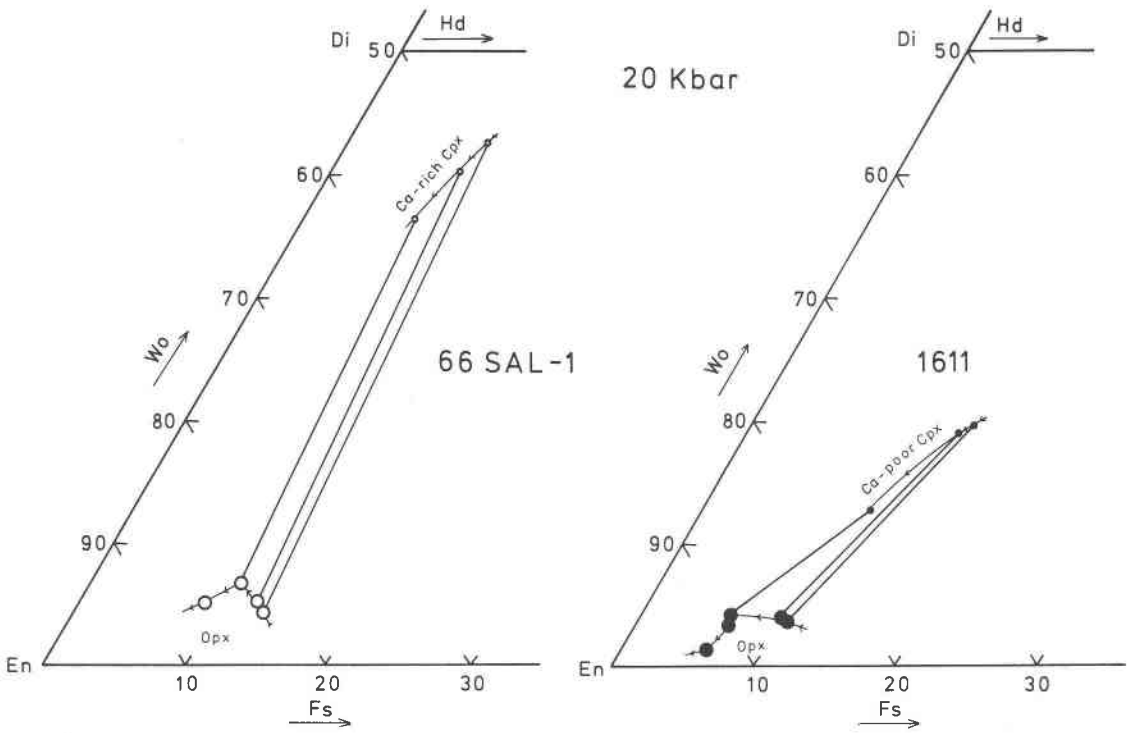

Fig. 7. Pyroxene quadrilateral showing coexisting pyroxenes of nodules 1611 and 66SAL-1 at 20 kbar.

nopyroxene (pigeonite) falls rapidly within the melting interval (Fig. 7), resulting in decreasing Ca content of the coexisting tholeiitic liquid. This situation contrasts with that for 66SAL-1, where the coexisting clinopyroxene is diopsidic and of relatively constant Ca content throughout the melting interval. The liquids of 66SAL-1 coexisting with clinopyroxene do not change their Ca contents significantly (Table 3).

Quality chemical analyses of liquids at 35 kbar were unattainable owing to quenching problems. However, a few semiquantitative analyses inside the olivine + garnet + 2 pyroxene assemblage suggest alkali picrite composition. At successively higher temperatures, phase assemblages at 35 kbar are similar to those of 1611 at 20 kbar starting from its solidus (Fig. 3), suggesting that the liquids in these melting ranges are similar as well. The 35 kbar melting range of nodule 1611 would produce four distinct regions. The first 25 percent melt is alkali picritic (in the presence of garnet), followed by olivine tholeiitic from 25 to 45 percent melting (in the presence of olivine and two pyroxenes), followed by picritic from 45 to about 75 percent melting (olivine + orthopyroxene) and finally komatiite-type liquids in the highest-temperature melting range, where olivine is the only coexisting crystalline phase.

Discussion

Each melting range of peridotite, involving a specific phase assemblage and a well-defined temperature range, defines a specific melt composition that varies only within narrow compositional limits. The width of these melting ranges depends on peridotite compositions, inasmuch as the bulk composition of peridotite is expressed by the proportions of peridotite minerals. In this sense, complex natural peridotite rocks behave similarly to model systems used to describe melting behavior of peridotite in the upper mantle.

The initial melting range (most closely resembling invariant) comprises 25 percent or more melt. At pressures below the stability field of garnet, the liquid of the initial 25 percent or more melting resembles olivine tholeiite composition. This liquid coexists with olivine, 2 pyroxenes (orthopyroxene and pigeonitic clinopyroxene in 1611; orthopyroxene and diopsidic clinopyroxene in 66SAL-1), and spinel. From neither sample can tholeiitic liquid be described by its four coexisting phases. Consequently, liquids of both samples have a reaction relation to their coexisting spinel peridotite residue. Reaction relations in volatile-free model peridotite were studied by Kushiro (1969) and by Kushiro and Yoder (1974) in the sys-

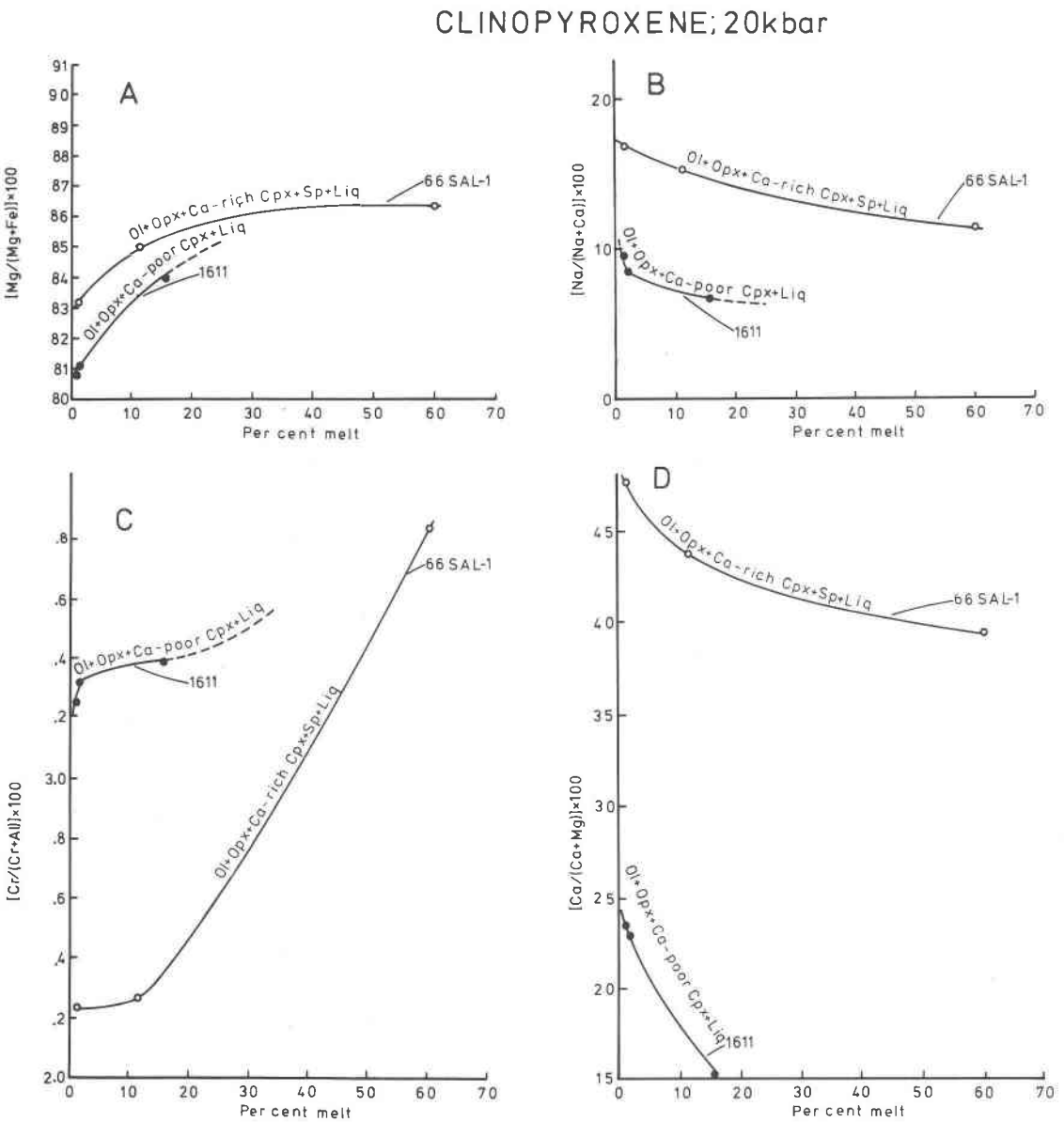

Fig. 8. Chemical trends of clinopyroxenes as a function of degree of melting. Mineral assemblages describe coexisting phases in melting intervals.

tem $MgSiO_3$–$CaSiO_3$–Al_2O_3. On the basis of these studies, two reaction relations can be deduced for the two nodules. The lower-temperature melting range of 66SAL-1 generates tholeiitic liquid by the reaction

$$Opx + Cpx + Sp \rightleftarrows Ol + Liq_1. \quad (2)$$

In the higher-temperature melting range of nodule 1611, the clinopyroxene is pigeonite, and the melting reaction is

$$Ol + Cpx \rightleftarrows Opx + Liq_2 \quad (3)$$

As would be expected from the data of Kushiro and Yoder (1974), reaction 2 occurs at lower temperature (see Fig. 1) and generates a liquid (Liq_1) with a slightly higher Ca and Al content than that of Liq_2 (reaction 3) (Table 3). Unfortunately, liquid compositions could not be obtained from the 35 kbar garnet-bearing runs. This pressure of 35 kbar is within the range where the data on the simple $CaSiO_3$–$MgSiO_3$–Al_2O_3 system (Kushiro and Yoder, 1974) suggest the reaction

Table 3. Compositions of liquids at 20 kbar

Starting Material:	1611	1611	1611	1611	1611	1611*	1611*	66SAL-1	66SAL-1
Temp. (°C):	1450	1475	1500	1525	1550	1600	1700	1360	1375
SiO_2	43.80	44.60	50.20	49.60	50.99	48.70	46.30	41.80	47.70
TiO_2	1.40	1.00	0.80	0.70	0.70	0.60	0.40	0.80	0.80
Al_2O_3	12.70	12.20	12.20	9.10	8.80	6.10	4.50	15.80	12.30
FeO†	13.70	12.50	9.60	9.70	12.20	17.80	14.60	9.80	7.90
MnO	0.30	0.20	0.30	0.20	0.10	0.10	0.10	0.20	0.20
MgO	12.00	14.30	13.80	19.60	15.70	18.50	27.40	19.90	17.80
CaO	13.70	13.20	10.70	9.20	9.3	7.20	5.30	10.10	12.10
Na_2O	1.40	1.10	1.50	0.90	1.3	0.70	0.50	0.90	0.80
K_2O	0.60	0.50	0.60	0.50	0.3	0.30	0.20	0.10	0.20
Totals	99.60	99.60	99.70	99.50	99.40	100.00	99.30	99.40	99.80
				Cationic Norm					
Or	1.81	2.94	3.51	2.89	1.59	1.77	1.14	0.40	0.98
Ab	0	1.94	13.32	7.89	12.08	6.26	4.33	1.70	6.83
An	26.70	26.73	24.52	18.86	17.05	12.58	9.11	37.60	28.75
Ne	7.57	4.73	0	0	0	0	0	3.72	0
Lc	1.40	0	0	0	0	0	0	0	0
Cpx	33.22	30.72	22.40	20.57	23.00	18.42	13.00	8.52	23.87
Opx	0	0	18.98	25.66	32.59	35.07	23.84	0	12.36
Ol	27.34	31.56	16.18	23.18	12.76	25.06	48.03	46.97	26.19
Il	1.96	1.39	1.10	0.95	0.94	0.83	0.54	1.08	1.02

Starting Material:	66SAL-1	1611+ H_2O	1611+ H_2O	1611+ H_2O	1611+ H_2O	1611+ H_2O*	1611+ H_2O*	1611+ H_2O
Temp. (°C):	1400	1460	1475	1500	1525	1550	1600	1750
SiO_2	46.80	45.10	46.70	48.40	46.30	46.40	47.00	46.10
TiO_2	0.90	1.10	0.90	0.90	0.50	0.40	0.40	0.40
Al_2O_3	12.60	11.00	10.40	10.70	7.50	4.80	4.60	4.40
FeO†	8.80	13.60	13.40	12.00	12.20	13.90	13.80	13.70
MnO	0.20	0.30	0.20	0.20	0.30	0.10	0.20	0.10
MgO	16.30	13.70	16.00	13.30	23.40	27.60	28.00	29.50
CaO	12.60	13.40	9.90	12.70	8.00	5.40	5.40	5.10
Na_2O	1.20	1.10	1.50	1.30	0.90	0.60	0.60	0.50
K_2O	0.10	0.50	0.60	0.50	0.40	0.20	0.20	0.20
Totals	99.50	99.80	99.60	100.00	99.50	99.40	100.20	100.00
				Cationic Norm				
Or	0.58	3.19	3.39	2.89	2.46	1.36	1.30	1.23
Ab	10.56	2.77	13.50	11.45	8.07	5.00	4.87	4.51
An	28.15	23.51	19.63	21.92	14.51	9.40	8.87	8.51
Ne	0	4.21	0	0	0	0	0	0
Lc	0	0	0	0	0	0	0	0
Cpx	26.53	34.34	23.17	32.68	19.07	13.07	13.32	12.38
Opx	1.87	0	1.07	5.95	8.24	21.67	23.15	18.91
Ol	31.08	30.56	38.04	23.91	46.96	48.96	47.93	53.94
Il	1.23	1.42	1.20	1.21	0.70	0.70	0.56	0.52

*Liquid composition calculated from mass balance (proportions of olivine and coexisting liquid are known).
†Total iron as FeO.

$$Ga + Opx + Cpx \rightleftarrows Ol + Liq \qquad (4)$$

to describe the initial melting of the natural peridotites.

At 20 kbar, about 25 percent melting of nodule 1611 is obtained at the invariant point described by reaction 3. As the temperature is increased further, the partial melt composition from nodule 1611 moves down along an olivine–orthopyroxene liquidus surface and finally into the liquidus volume of olivine. Similar reasoning applies to nodule 66SAL-1. As much as 60 percent melt can be generated at the invariant point of nodule 66SAL-1, suggesting that this composition was itself generated at such an invariant point and therefore is not a parent but a product of partial melting in the upper mantle.

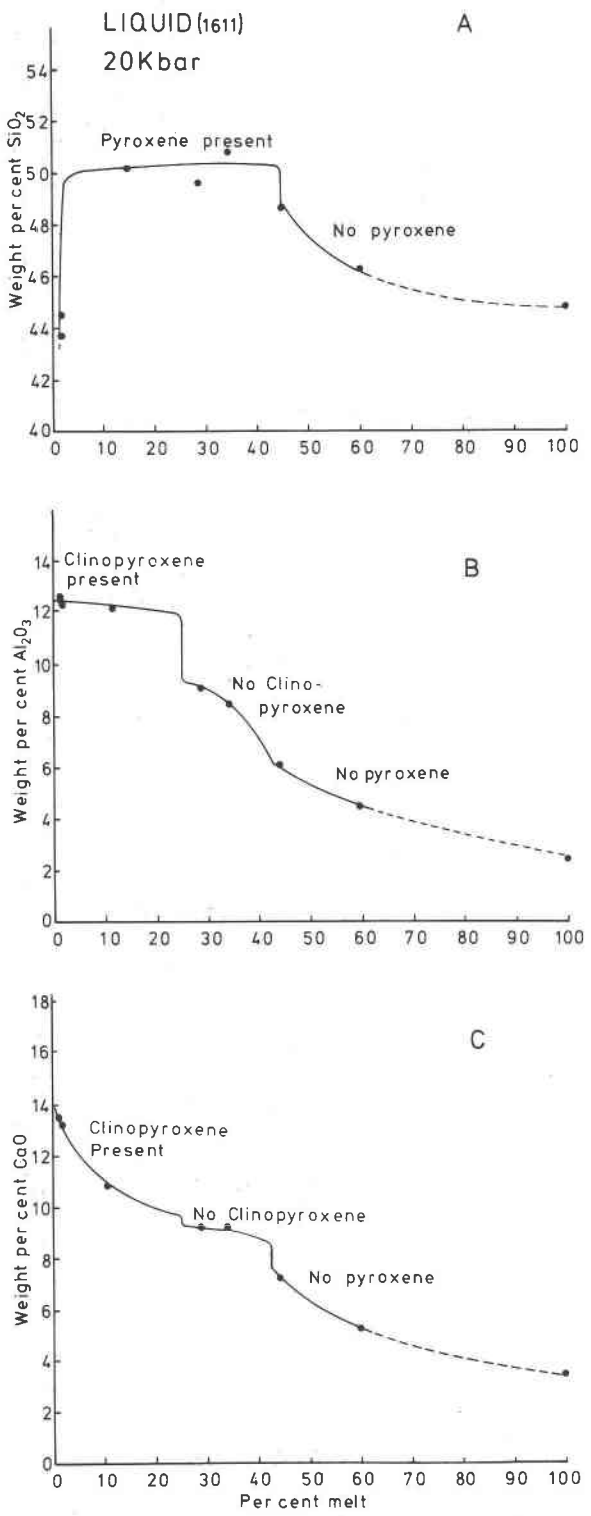

Fig. 9. Chemical trends of liquids as a function of degree of melting. Mineral assemblages describe coexisting phases in melting intervals.

In summary, the partial melts are compositionally controlled by their coexisting silicate minerals. In the spinel stability field, only three liquid compositions can be obtained by partial melting of volatile-free peridotite—olivine tholeiite, picrite, and peridotitic komatiite. Within the stability field of garnet peridotite there are four types of liquids—alkali picrite, olivine tholeiite, picrite, and peridotitic komatiite. Clearly, a grid based simply on numerical manipulation of proportions of minerals (as summarized by Green, 1970) does not adequately describe the melting behavior of volatile-free peridotite in the upper mantle.

Acknowledgments

Critical reviews by Drs. F. R. Boyd, E. F. Osborn, R. V. Danchin, and H. S. Yoder, Jr., are greatly appreciated.

References

Anderson, A. T. (1975) Some basaltic and andesitic gases. *Rev. Geophys., 13,* 37–57.

Boettcher, A. L., B. O. Mysen and P. J. Modreski (1975) Phase relationships in natural synthetic peridotite–H_2O and peridotite–H_2O–CO_2 systems at high pressure. *Phys. Chem. Earth, 9,* 955–968.

Bottinga, Y. and D. F. Weill (1972) The viscosity of magmatic silicate liquids: a model for calculation. *Am. J. Sci., 272,* 438–475.

Bowen, N. L. (1928) *Evolution of the Igneous Rocks.* Princeton University Press, Princeton, N. J.

Boyd, F. R. and J. L. England (1960) Apparatus for phase equilibrium measurements at pressures up to 50 kilobars and temperatures up to 1750°C. *J. Geophys. Res., 65,* 741–748.

Eggler, D. H. (1974) Effect of CO_2 on the melting of peridotite. *Carnegie Inst. Wash. Year Book, 73,* 215–224.

——— (1975) Peridotite–carbonatite relations in the system MgO–SiO_2–CO_2. *Carnegie Inst. Wash. Year Book, 74,* 468–474.

Green, D. H. (1970) A review of experimental evidence on the origin of basaltic and nephelinitic magmas. *Phys. Earth Planet. Interiors, 3,* 221–235.

——— and A. E. Ringwood (1967) The genesis of basaltic magmas. *Contrib. Mineral. Petrol., 15,* 103–190.

Irving, A. J. and P. J. Wyllie (1975) Subsolidus and melting relationships for calcite, magnesite and the join $CaCO_3$–$MgCO_3$ to 36 kb. *Geochim. Cosmochim. Acta, 39,* 35–53.

Hensen, B. J. (1973) Pyroxenes and garnets as geothermometers and geobarometers. *Carnegie Inst. Wash. Year Book, 72,* 527–534.

Jackson, E. D. and T. L. Wright (1970) Xenoliths in the Honolulu volcanic series, Hawaii. *J. Petrol., 11,* 405–430.

Kushiro, I. (1969) The system forsterite–diopside–silica with and without water at high pressures. *Am. J. Sci., 267-A,* 269–294.

——— (1972) Effect of water on the composition of magmas formed at high pressures. *J. Petrol., 13,* 311–334.

——— (1973) Partial melting of garnet–lherzolite from kimberlite at high pressures. In P. H. Nixon, Ed., *Lesotho Kimberlites,* p. 294–300. Lesotho National Development Corp., Maseru.

——— and Y. Nakamura (1970) Equilibrium relations of hypersthene, pigeonite and augite in crystallizing magmas: microprobe

study of a pigeonite andesite from Weiselberg, Germany. *Am. Mineral., 55,* 1999–2016.

——— and H. S. Yoder, Jr. (1970) Stability of iron-free pigeonite in the system $MgSiO_3$–$CaMgSi_2O_6$. *Carnegie Inst. Wash. Year Book, 68,* 226–229.

——— and ——— (1974) Formation of eclogite from garnet lherzolite: liquidus relations in a portion of the system $MgSiO_3$–$CaSiO_3$–Al_2O_3 at high pressure. *Carnegie Inst. Wash. Year Book, 73,* 266–269.

———, ——— and B. O. Mysen (1976) Viscosity of basalt and andesite magmas at high pressures. *EOS, 57,* 354.

———, ——— and M. Nishikawa (1968) Effect of water on the melting of enstatite. *Geol. Soc. Am. Bull., 79,* 1685–1692.

Merrill, R. B., J. K. Robertson and P. J. Wyllie (1970) Melting reactions in the system $NaAlSi_3O_8$–$KAlSi_3O_8$–SiO_2–H_2O to 20 kilobars compared to results from other feldspar–quartz–H_2O and rock–H_2O systems. *J. Geol., 78,* 558–570.

Mysen, B. O., R. J. Arculus and D. H. Eggler (1975) Solubility of carbon dioxide in natural nephelinite, tholeiite and andesite melts to 30 kbar pressure. *Contrib. Mineral. Petrol., 53,* 227–239.

——— and A. L. Boettcher (1975a) Melting of a hydrous mantle. I. Phase relations of natural peridotite at high pressures and temperatures with controlled activities of water, carbon dioxide and hydrogen. *J. Petrol., 16,* 520–548.

——— and ——— (1975b) Melting of a hydrous mantle. II. Geochemistry of crystals and liquids formed by anatexis of mantle peridotite at high pressures and temperatures as a function of controlled activities of water, hydrogen and carbon dioxide. *J. Petrol., 16,* 549–592.

———, D. H. Eggler, M. G. Seitz and J. R. Holloway (1976) Carbon dioxide in silicate melts and crystals. I. Solubility measurements. *Am. J. Sci., 276,* 455–479.

——— and M. G. Seitz (1975) Trace element partitioning determined by beta-track mapping: an experimental study using carbon and samarium as examples. *J. Geophys. Res., 80,* 2627–2635.

Nixon, P. H. and F. R. Boyd (1973) Petrogenesis of the granular and sheared ultrabasic nodule suite in kimberlites. In P. H. Nixon, Ed., *Lesotho Kimberlites,* p. 48–56. Lesotho National Development Corp., Maseru.

Shaw, H. R. and E. D. Jackson (1973) Linear island chains in the Pacific: results of thermal plumes or gravitational anchors? *J. Geophys. Res., 78,* 8634–8652.

Shimizu, N. (1974) Rare earth elements (REE) in garnets and clinopyroxenes from garnet lherzolite nodules in kimberlite. *Carnegie Inst. Wash. Year Book, 73,* 954–961.

Waff, H. S. (1975) Pressure-induced coordination changes in magmatic liquids. *Geophys. Res. Lett., 2,* 193–196.

Yoder, H. S., Jr. (1976) *Generation of Basaltic Magma.* National Academy of Sciences, Washington, D. C.

Manuscript received, October 7, 1976; accepted for publication April 19, 1977.